# Continuous direct compression: Development of an empirical predictive model and challenges regarding PAT implementation

B. Bekaert [a], B. Van Snick [b], K. Pandelaere [a], J. Dhondt [b], G. Di Pretoro [b], T. De Beer [c], C. Vervaet [a], V. Vanhoorne [a,*]

[a] Laboratory of Pharmaceutical Technology, Department of Pharmaceutics, Ghent University, Ottergemsesteenweg 460, B-9000 Ghent, Belgium
[b] Oral Solid Dosage, Drug Product Development, Discovery Product Development and Supplies, Pharmaceutical Research and Development, Division of Janssen Pharmaceutica, Johnson & Johnson, Turnhoutseweg 30, B-2340 Beerse, Belgium
[c] Laboratory of Pharmaceutical Process Analytical Technology, Department of Pharmaceutical Analysis, Ghent University, Ottergemsesteenweg 460, B-9000 Ghent, Belgium

## A R T I C L E   I N F O

## A B S T R A C T

In this study, an empirical predictive model was developed based on the quantitative relationships between blend properties, critical quality attributes (CQA) and critical process parameters (CPP) related to blending and tableting. The blend uniformity and API concentration in the tablets were used to elucidate challenges related to the processability as well as the implementation of PAT tools. Thirty divergent ternary blends were evaluated on a continuous direct compression line (ConsiGma™ CDC-50). The trials showed a significant impact of the impeller configuration and impeller speed on the blending performance, whereas a limited impact of blend properties was observed. In contrast, blend properties played a significant role during compression, where changes in blend composition significantly altered the tablet quality. The observed correlations allowed to develop an empirical predictive model for the selection of process configurations based on the blend properties, reducing the number of trial runs needed to optimize a process and thus reducing development time and costs of new drug products. Furthermore, the trials elucidated several challenges related to blend properties that had a significant impact on PAT implementation and performance of the CDC-platform, highlighting the importance of further process development and optimization in order to solve the remaining challenges.

## 1. Introduction

In recent years the pharmaceutical industry invested a lot in the application of continuous manufacturing as the main production technique to increase the efficiency and flexibility of manufacturing (Lee et al., 2015). Improvements in lead-time, in-line process control, process understanding and equipment footprint are some of the advantages of switching from batch to continuous manufacturing (Ierapetritou et al., 2016; Nasr et al., 2017; Schaber et al., 2011). Compression, a widely used production technique in the pharmaceutical industry, is one of the frontrunners in the shift to a fully integrated continuous process. Its inherent continuous nature, combined with the potential of the preceding unit operations (i.e. feeding and blending) to be performed in a continuous fashion, were the basis for the development of several

---

continuous direct compression (CDC) – lines. Manual dispensing transformed into loss-in-weight (LIW) feeding, while batch blenders evolved into linear convective paddle blenders. These steps resulted in 2014 in the development of the first fully integrated continuous direct compression (CDC) line by GEA (i.e. ConsiGma® CDC-50), with many customized lines being implemented in several companies (e.g. Vertex Pharmaceuticals, Janssen, Merck, Pfizer, …). Shortly after, Glatt and Fette Compacting combined their expertise in order to develop, in 2017, a CM line where a linear continuous Glatt blender was combined with a Fette FE35 rotary tablet press (Manufacturing Chemist, 2017). Furthermore, L.B. Bohle developed the QbCon® 25 platform, containing a direct compression unit, combining Gericke feeders and blenders with a Korsch Tablet press (Bohle, 2019). This emergence of equipment for continuous manufacturing of solid dosage forms already resulted in the FDA approval of seven drug products manufactured in a continuous manner. The first ever continuously manufactured product Orkambi®, produced by Vertex Pharmaceuticals, saw its approval in July 2015. Soon after, Johnson & Johnson successfully switched Prezista® from batch to continuous through an intensive collaboration between J&J, Rutgers University and the University of Puerto Rico (Pharmaceutical Technology, 2016). In 2017, Eli Lilly's Verzenio® received its approval to be manufactured in a continuous way (Eli Lilly, 2018). The following year was a very fruitful year for continuous manufacturing with the approval of two products manufactured by Pfizer (i.e. Daurismo® and Lorbrena®) and the second approved drug product from Vertex Pharmaceuticals (Portier et al., 2020; U.S. Food and Drug Administration, 2018a; U.S. Food and Drug Administration, 2018b; U.S. Food and Drug Administration, 2018c). Finally, Vertex Pharmaceuticals registered their third continuously manufactured drug product Trikafta® (2019) (U.S. Food and Drug Administration, 2019).

Due to the criticality of each unit operation, a growing body of literature was developed by several research groups. During the first unit operation (i.e. continuous feeding), any occurring deviation or problem could be passed down through the line, potentially affecting the final product quality. Therefore, extensive experimental work was performed where the feeding of raw materials was investigated and optimized (Engisch and Muzzio, 2014; Van Snick, 2019; Van Snick et al., 2019; Bostijn et al., 2019; Bekaert et al., 2021a, 2021c). For the blending step, both experimental and modeling work has been done, investigating an influence of material properties, process settings and blender configurations on the blending performance (Pernenkil and Cooney, 2006; Portillo et al., 2008; Gao et al., 2011; Osorio and Muzzio, 2016; Bekaert et al., 2021b). The final and important compaction step, used both in batch and continuous, has been investigated extensively resulting in large numbers of literature reports ranging from experimental to conceptual topics (Patel et al., 2006; Peeters et al., 2018; Van Snick et al., 2018). Furthermore, the implemented Process Analytical Technology (PAT) tools could increase process knowledge as well as enable real-time release testing through continuous product quality monitoring (i.e. blend/content uniformity) (Pawar et al., 2016). Next to the literature describing each unit operation separately, a handful of papers reported work on an integrated from powder-to-tablet CDC line (Järvinen et al., 2013a; Järvinen et al., 2013b; Simonaho et al., 2016; Van Snick et al., 2017a; Van Snick et al., 2017b; García-Muñoz et al., 2017; Roth et al., 2017; Galbraith et al., 2020; Galbraith et al., 2019).

Based on the available literature, most of the knowledge regarding continuous direct compression comes from research performed on one specific unit operation. The studies investigating an integrated from powder-to-tablet CDC line most often focused on a specific formulation and did not quantify specific correlations between the materials and CDC responses. Furthermore, up-to-now no empirical predictive models have been developed for a fully integrated CDC line for a wide variety of materials. Therefore, 30 ternary blends were processed on a fully integrated CDC line with the aim of finding quantitative relationships between blend properties, critical quality attributes (CQA) and critical process parameters (CPP) related to blending (i.e. hold-up mass, residence time, strain, impeller speed, impeller configuration) and tableting (i.e. tablet weight variability, fill depth, tablet press settings) performance. Based on Partial Least Squares (PLS) regression, an empirical predictive model was developed in order to select process configurations for a specific formulation based on the blend properties. Furthermore, blend and content uniformity measurements helped to determine the processability challenges of divergent blends as well as challenges related to the implementation of PAT equipment into a continuous line. This study is an extension of the long-term feeding paper discussing the data generated during these trials (Bekaert et al., 2021c).

## 2. Materials

Table 1 gives an overview of the selected materials, including the supplier information and references to the abbreviations used in the paper.

## 3. Equipment

The study was performed on a ConsiGma® CDC-50 (GEA, Wommelgem, Belgium). The fully integrated continuous line consists of material handling, loss-in-weight (LIW) feeding, two consecutive continuous blenders (i.e. main and lubricant blender), a rotary tablet press and in-line NIR equipment (Fig. 1), which has been extensively described by Van Snick et al. (2017a, 2017b).

### 3.1. Material handling and loss-in-weight feeding

The ConsiGma® CDC-50 is equipped with Compact Feeders (CF) which can be integrated at blender inlet 1 (i.e. main blender) and blender inlet 2 (i.e. lubricant blender). Feeders at the main blender inlet (i.e. 6 available locations) are used for materials requiring intensive mixing, while the lubricant blender inlet (i.e. 2 available feeder locations) can be used for shear-sensitive materials or materials requiring limited mixing. In total, 6 feeders can be active at the same time (e.g. 5 at the main blender inlet and 1 at the lubricant blender inlet).

Each LIW feeder is equipped with a dedicated material handling unit consisting of either a conical hopper with a level sensor (3.2 L) or a cylindrical feed tube (7 L), used for vacuum or gravity-controlled top-ups respectively. The gravity-controlled material handling unit is preferred for highly cohesive powders or powders that are sensitive to triboelectric charging during the vacuum transport. Furthermore, the material handling unit is equipped with a pneumatic vibrator (Volkmann, Soest, Germany) to improve the processability of adhesive or poorly flowing materials. A rotating bowl-valve with adjustable volumes (i.e. 0.4; 0.8; 1.2 or 1.6 L) is installed at the bottom of the material handling unit in order to control the hopper refill of the Compact Feeder.

**Table 1**
Overview of selected materials.

| Material | Supplier | Code |
|---|---|---|
| Paracetamol powder | Mallinckrodt | P_P |
| Paracetamol dense powder | Mallinckrodt | P_DP |
| Paracetamol micronized | Mallinckrodt | P_μ |
| Caffeine anhydrous powder | BASF | C_P |
| Metoprolol tartrate micronized | Utag | MPT_μ |
| Theophylline anhydrous powder | Siegfried | T_P |
| Spray dried API | Janssen | API_sd |
| Pearlitol 100 SD | Roquette | SD100 |
| Emcompress AN | JRS | DCP |
| Avicel PH-101 | FMC | PH101 |
| Avicel PH-200 | FMC | PH200 |
| Tablettose 80 | Meggle | T80 |
| Ligamed MF-2-V | Peter Greven | MgSt |
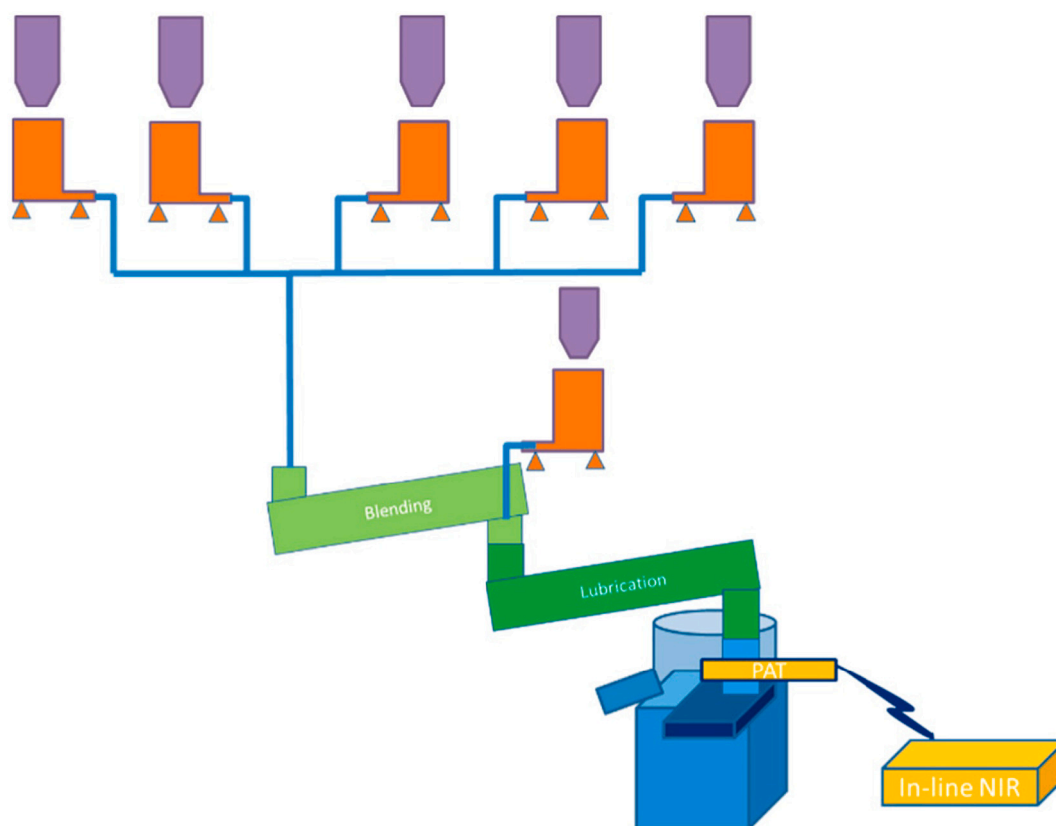
**Fig. 1.** Flowsheet of the CDC-50. Material handling (purple), loss-in-weight feeding (orange), main blender (light green), lubrication (dark green), feed tube (light blue), in-line NIR equipment (yellow) and rotary tablet press (blue). Figure reprinted from Van Snick et al. (2017a) with permission of Elsevier.

### 3.2. Blending unit

The blending unit consists of two consecutive cylindrical dry powder blenders. Both the main and lubricant blender contain a rotating impeller positioned in an upwards tilted angle of 15°. The impeller consists of a central shaft with 60 adjustable blades. Depending on the position of the blades, they can function as either transport or radial mixing blades. Transport blades are oriented at 45° along the axis of the shaft, while radial mixing blades have an angle of 0° along the axis of the shaft. The impeller speed can be varied between 45 and 450 rpm.

### 3.3. Rotary tablet press

After blending, the blend moves through a feed tube into the feed frame of the tablet press (MODUL™ S, GEA, Halle, Belgium). Inside the feed tube a level sensor is installed, maintaining a constant fill level during manufacturing. A fiber optic contact probe (Lighthouse™ probe, GEA, Wommelgem, Belgium) connected with an NIR spectrometer (Tidas P analyzer, J&M Analytik, Essingen, Germany) was integrated just above the feed frame inlet, allowing the collection of spectra every second. The MODUL™ S tablet press was equipped with moving rollers at the pre-compression station and fixed rollers at the main compression station.

### 4. Methods

#### 4.1. Blend selection and characterization

Thirty ternary blends were selected, containing an API (9.93% *w*/w), a filler (89.32% w/w) and magnesium stearate (MgSt) as a lubricant (0.75% w/w). The APIs and fillers comprising the blends were picked based on the selection as described in a previous paper on long-term

feeding characterization from our group (Bekaert et al., 2021c). In order to challenge the blend uniformity while maintaining NIR sensitivity (i.e. lowest possible API concentration that is still accurately measured via NIR), a 10/90 API/filler ratio was chosen. The blend ratio for blends containing Pearlitol 100 SD (SD100) was changed in order to increase the down-stream tabletability (i.e. 9.93/88.82/1.25 – ratio). An overview of the ternary blends is given in Table 2.

The off-line prepared blends (blending protocol: 25 min at 25 rpm for the API/filler-mixture, followed by 5 min at 15 rpm for the API/filler/ MgSt mixture, using a tumble blender (Inversina, Bioengineering, Wald, Switzerland)), were characterized for a selection of potentially relevant descriptors during the blending and tableting step of continuous direct compression. The different characterization methods were performed using the protocols described by Van Snick et al. (2018). Table 3 displays the descriptors, their abbreviation and applied characterization methods.

#### 4.2. CDC-50 trial runs

##### 4.2.1. Experimental setup

The impact of varying blend compositions on the processability at different main blender configurations (i.e. shear zone in the middle of the impeller with 4, 10 or 16 radial mixing blades) and speeds (i.e. 200, 300 or 400 rpm) was studied. The throughput (i.e. 20 kg/h), lubricant blender configuration (i.e. no radial mixing blades) and impeller speed (i.e. 200 rpm) remained fixed throughout the study. The MODUL™ S tablet press was equipped with 38 flat-face bevel-edge 8 mm EURO B punches with breaking line and the turret speed was set at 50 rpm, resulting in a target tablet weight of 175 mg. The speed of the paddles in the feed frame were kept at a fixed value throughout the experiments (i. e. 58 rpm and 70 rpm for paddle 1 and 2, respectively). A pre-compression force (PCF) of 1.5kN with minimal displacement (PCD)

**Table 2**
Overview of the ternary blends.

| Blend | API | Filler | Lubricant |
|---|---|---|---|
| F1 | P_μ | SD100 | MgSt |
| F2 | P_P | | |
| F3 | P_DP | | |
| F4 | C_P | | |
| F5 | API_sd | | |
| F6 | MPT_μ | | |
| F7 | P_μ | DCP | MgSt |
| F8 | P_P | | |
| F9 | P_DP | | |
| F10 | C_P | | |
| F11 | API_sd | | |
| F12 | MPT_μ | | |
| F13 | P_μ | PH101 | MgSt |
| F14 | P_P | | |
| F15 | P_DP | | |
| F16 | C_P | | |
| F17 | API_sd | | |
| F18 | MPT_μ | | |
| F19 | P_μ | T80 | MgSt |
| F20 | P_P | | |
| F21 | P_DP | | |
| F22 | C_P | | |
| F23 | API_sd | | |
| F24 | MPT_μ | | |
| F25 | P_μ | PH200 | MgSt |
| F26 | P_P | | |
| F27 | P_DP | | |
| F28 | C_P | | |
| F29 | API_sd | | |
| F30 | MPT_μ | | |

**Table 3**
Overview of blend descriptors and their respective abbreviation, adopted from Van Snick et al. (2018).

| Characterization method | Descriptor | Abbreviation |
|---|---|---|
| Flowpro | Flow through an orifice (= Flowrate) | FP |
| FT4 powder rheometer | Compressibility (at 15 kPa), b from Kawakita equation | C_15kPa, b |
| | Conditioned bulk density | CBD |
| | Permeability at 15 kPa | k_15kPa |
| | Susceptibility of permeability to Compressibility Index (slope) | k_CI_Sus |
| Helium pycnometry | True density, porosity | ρtrue, ε |
| Tapping device | Bulk and tapped density | ρb, ρt |
| | Compressibility Index | CI |
| Ring shear tester | Angle of internal friction, angle of internal friction steady state flow, effective angle of internal friction | φlin, φsf, φe |
| | Cohesion | τc |
| | Consolidated density-weighed flow | ffρ |
| | Flow function coefficient, major principal stress, unconfined yield stress | ffc, MPS, UYS |
| | Wall friction angle | WFA_S |

(i.e. 0.1 mm) and a main compression force (MCF) of 5kN were applied. Tablet press control loops were deactivated, hence adjustments to the fill depth (FD) and compression roller heights were required to reach the setpoints.

Prior to start-up, the feeders were primed (i.e. filling of the screws for 5 to 10 s) and the top-up systems filled. During the start-up phase ($\pm$ 15 min), tablet press settings (i.e. fill depth, pre-compression and main compression height) were adjusted in order to reach the required tablet weight and compression forces. Once steady state conditions were reached, the process was run for 15 min to obtain sufficient blend uniformity measurements. Steady state was achieved when limited feed tube level variability was seen, meaning that the blenders reached a stable fill level and the feeders and tablet press had a matching flow rate.

Furthermore during steady state, tablets were collected for 6 min and 40 s according to a sample plan. The sample plan consisted of 40 grab samples, each with 10 s sampling. Afterwards, the steady state process was stopped instantaneously and the shut-off valves at the end of each blender were closed. The remaining powder in each of the blenders was collected pneumatically in order to determine the hold-up mass. Data-logging was performed by the integrated CDC-50 software (GEA, Wommelgem, Belgium) and external NIR software (SentroPAT FO, Sentronic, Dresden, Germany).

*4.2.2. CDC-50 responses*

Data was collected from each unit operation with an overview of the different unit operations and NIR tools, their corresponding responses and abbreviations given in Table 4.

*4.2.2.1. Feeding responses.* Every second, feeder data was recorded by the data recording system of the GEA compact feeder. The feeder screw speed (rpm), net weight (g), mode of operation (volumetric or gravimetric), mass flow rate (g/s) and feed factor (g/revolution) were used to investigate the gravimetric feeding performance. The results and conclusions of the acquired data are discussed in detail in Bekaert et al. (2021c).

*4.2.2.2. Blending responses.* The CDC line was instantaneously stopped during steady state in order to collect the powder present in both blenders. Based on the amount of powder in the blenders, the hold-up mass for the main and lubricant blender ($HM_1$ and $HM_2$, respectively) was determined. Using Eqs. (1) and (2), the bulk residence time (BRT) and strain experienced by the powder in the blender (number of blade passes; #BP) were calculated:

$$BRT\ (s) = \frac{HM\ (g)}{Throughput\ \left(\frac{g}{s}\right)} \tag{1}$$

$$\#BP = BRT\ x\ \frac{Impeller\ speed\ (rpm)}{60} \tag{2}$$

*4.2.2.3. Compression responses.* Once the tablet press settings were optimized to reach the required tablet weight and compression force, the values for fill depth, pre-compression and main compression height (PCH and MCH) were collected. During steady state conditions, values for the pre-compression displacement, the variability in the

**Table 4**
Overview of CDC-50 unit operations and NIR tools, their corresponding responses and used abbreviation.

| Unit operation | Response | Abbreviation |
|---|---|---|
| LIW feeder | Screw speed (rpm) | SS |
| | Powder net weight (g) | nw |
| | Mass flow rate (g/s) | MF |
| | Feed factor (g/revolution) | FF |
| Main and lubricant blender | Main blender hold-up mass (g), lubricant blender hold-up mass (g) | $HM_1$, $HM_2$ |
| | Bulk residence time main blender (s) | $BRT_1$ |
| | Number of blade passes main blender | $\#BP_1$ |
| | Fill depth (mm) | FD |
| Compression station | Main compression height (mm), pre-compression height (mm) | MCH, PCH |
| | Main compression force variability (%) | $\sigma_{Force}$ |
| | Pre-compression displacement variability (%) | $\sigma_{PCD}$ |
| | Tablet weight variability (%) | $RSD_{TW}$ |
| | Tablet porosity | $\varepsilon_{Tablet}$ |
| SentroPAT FO probe/ Lighthouse™ probe | Blend uniformity (%), Label claim (%) | BU, LC |
| | Blend uniformity variability (%) | $RSD_{BU}$ |
| Antaris™ II FT-NIR Analyzer | Content uniformity (%), content uniformity variability (%) | CU, $RSD_{CU}$ |

displacement value ($\sigma_{PCD}$) and main compression force variability ($\sigma_{Force}$) were collected via the CDC-50 data-logging system.

The tablet grab samples taken during steady state were used to determine the tablet weight (g), hardness (N), thickness (mm) and diameter (mm). 20 tablets were randomly taken from each sample bag and analyzed using a semi-automatic tablet tester (SmartTest 50, Sotax, Basel, Switzerland). Based on these values, the tablet weight variability ($RSD_{TW}$) (Eq. (3)) and tablet porosity ($\varepsilon_{Tablet}$) (Eq. (4)) was calculated:

$$RSD_{TW}\ (\%) = \frac{\sqrt{\frac{\sum_{n}^{1}(TW - \overline{TW})2}{20}}}{\overline{TW}} \times 100 \tag{3}$$

with $\overline{TW}$ (g) the average tablet weight.

$$\varepsilon_{Tablet} = 1 - \frac{\rho_{app}}{\rho_{true}} \tag{4}$$

with $\rho_{app}$ the apparent density (i.e. tablet weight divided by its volume) and $\rho_{true}$ the true density of the blend.

### 4.2.3. Predictive model

Empirical predictive models were developed via Partial Least Squares (PLS) regression using the SIMCA 16 software (Umetrics, Umeå, Sweden). Two separate models were made in order to increase the goodness of fit ($R^2$) and predictive ability ($Q^2$). The first model, describing the long-term gravimetric feeding responses, was developed and discussed in a previous paper (Bekaert et al., 2021c). The second model regressed the CDC responses of the remaining unit operations (i.e. blending and compression) against the blend properties and process configurations for all processed blends. Prior to regression, unit variance (UV) scaling and mean centering was performed on the dataset and non-normally distributed responses were log transformed.

The model predictivity was externally validated with four additional ternary blends (Table 5). Two blends (i.e. F31 and F32) were composed of a new API (i.e. 9.93% theophylline anhydrous powder) combined with a cohesive or a dense filler (i.e. 89.32% PH101 or DCP, respectively) and 0.75% MgSt. The new API was chosen in order to investigate if the model was able to make predictions for unknown materials. The other two additional ternary blends (i.e. F33 and F34) had a known blend composition (i.e. P_DP/PH101/MgSt or P_DP/PH200/MgSt), but in a different ratio (i.e. 49.625/49.625/0.75%). This ratio was picked to challenge the model with blends where the higher API content could influence the processability. Prior to processing on the CDC-50, the off-line prepared blends were characterized for the same descriptors as the trial blends. Based on these values, the developed model predicted the required process settings and responses for the main blender and rotary tablet press. Next, the blends were processed at different main blender speeds (i.e. 200, 300 or 400 rpm) with a fixed impeller configuration (i.e. 10 radial mixing blades). Finally, a comparison between the predicted and observed values was made to determine how well the model could predict the required process settings and resulting responses. The comparison was performed by calculating the absolute and relative difference between the observed and predicted values (i.e. $Error_{Abs}$ and $Error_{Rel}$, respectively).

**Table 5**
Ternary blends used for external validation.

| Blend | API | Filler | Lubricant | API/filler/lubricant (%) |
|-------|------|--------|-----------|--------------------------|
| F31 | T_P | PH101 | MgSt | 9.93/89.32/0.75 |
| F32 | T_P | DCP | | |
| F33 | P_DP | PH101 | MgSt | 49.625/49.625/0.75 |
| F34 | P_DP | PH200 | | |

### 4.3. Blend uniformity

#### 4.3.1. Blend uniformity measurement

The blend uniformity (BU) was measured at two separate timepoints during continuous direct compression. The Lighthouse™ probe monitored the micro-mixing performance of the blenders in the feed tube at the outlet of the lubricant blender. The Lighthouse™ probe collected spectra every second in the spectral region from 1091 to 2107 nm with a pixel dispersion of 3.97 nm. Each spectrum was the average of 7 scans with an integration time of 60 ms. Considering the blend movement in the feed tube and estimated penetration depth of 0.5 mm (i.e. average measured penetration depth, taking changes in blend movement speed and density differences of the blends into consideration), each measurement corresponded with a sample size between 25 and 29 mg. The SentroPAT FO probe, integrated at the die filling position in the feed frame of the tablet press (i.e. via a fixed external frame with caliper to accurately set the 1 mm distance from the paddle wheel fingers) determined the blend uniformity just before the blend was compressed into tablets. Similar to the Lighthouse™ probe measurement, spectra were collected every second in the spectral region from 1091 to 2107 nm with a pixel dispersion of 3.97 nm. Each spectrum was the average of 10 scans with a 7 ms integration time. The fast moving and dense powder inside the feed frame, combined with a maximum penetration depth of approximately 1 mm, allowed to measure a sample size of approximately one unit dose (i.e. 175 mg). The collected spectra were loaded into the corresponding calibration models in order to get a prediction of the API content over time. Based on the predicted API concentrations, the label claim (LC) (%) was calculated (Eq. (5)):

$$LC\ (\%) = \frac{\text{Predicted API conc.}(\%)}{\text{Target API conc.}(\%)} \times 100 \tag{5}$$

#### 4.3.2. Blend uniformity calibration models

PLS regression models for each processed blend were constructed for both implemented NIR probes (i.e. SentroPAT FO and Lighthouse™ probe) allowing in-line monitoring of the API concentration during continuous direct compression. Five calibration standards for each blend (i.e. 4.97; 7.45; 9.93; 12.41; 14.9%) were measured using both probes, generating spectra used for the model development via SIMCA 16 software (Umetrics AB, Umeå, Sweden). The root mean squared error of cross validation (RMSEcv) of the models was used as an indicator for the model performance.

##### 4.3.2.1. Lighthouse™ probe.
The calibration standards were measured in-line through the addition of the standards to the feed tube above the feed frame inlet, mimicking the blend movement in the feed tube. The Lighthouse™ probe collected spectra every second in the spectral region from 1091 to 2107 nm with a pixel dispersion of 3.97 nm. Each spectra was the average of 7 scans with an integration time of 60 ms. The models were built by regressing the collected spectra (i.e. 5 calibration standards x 30 spectra) with the corresponding API concentration.

##### 4.3.2.2. SentroPAT FO probe.
The calibration standards for the SentroPAT FO probe were measured off-line by inserting the probe in bags containing the calibration standards. Every second spectra were collected in the spectral region from 1091 to 2107 nm with a pixel dispersion of 3.97 nm. Each spectrum was the average of 10 scans with a 7 ms integration time. Approximately 50 spectra, at different spots in the bag, were measured for each calibration standard, generating 250 off-line collected and pre-processed spectra. The calibration models were developed by regressing the measured spectra with their corresponding API concentration.

*International Journal of Pharmaceutics: X 4 (2022) 100110*

## 4.4. Content uniformity

### 4.4.1. Content uniformity measurement

The content uniformity (CU) was determined on a subset of sample bags collected during the trials (i.e. uneven numbered sample bags). Three random tablets from each sample bag (i.e. 3 × 20 sample bags) were measured using NIR transmission and loaded into the corresponding calibration models.

Content uniformity calibration models were developed using the calibration standards from the blend uniformity calibration models. The calibration standards were tableted using a Modul™ P tablet press (GEA, Halle, Wommelgem) at similar tablet press settings (i.e. PCD, PCF and MCF) seen during the trials. Each calibration tablet was made in three different thicknesses (i.e. based on the minimal, average and maximal tablet thickness for each formulation, seen during the CDC-trials) in order to take the variability in tablet thickness into consideration. The thickness was varied by adjusting FD. Five tablets from each set of calibration tablets were measured using NIR transmission (Antaris™ II FT-NIR Analyzer, Thermo Fisher Scientific, Waltham, USA) in the spectral region from 833.47 to 1333.16 nm with a spacing of 3.86 nm.
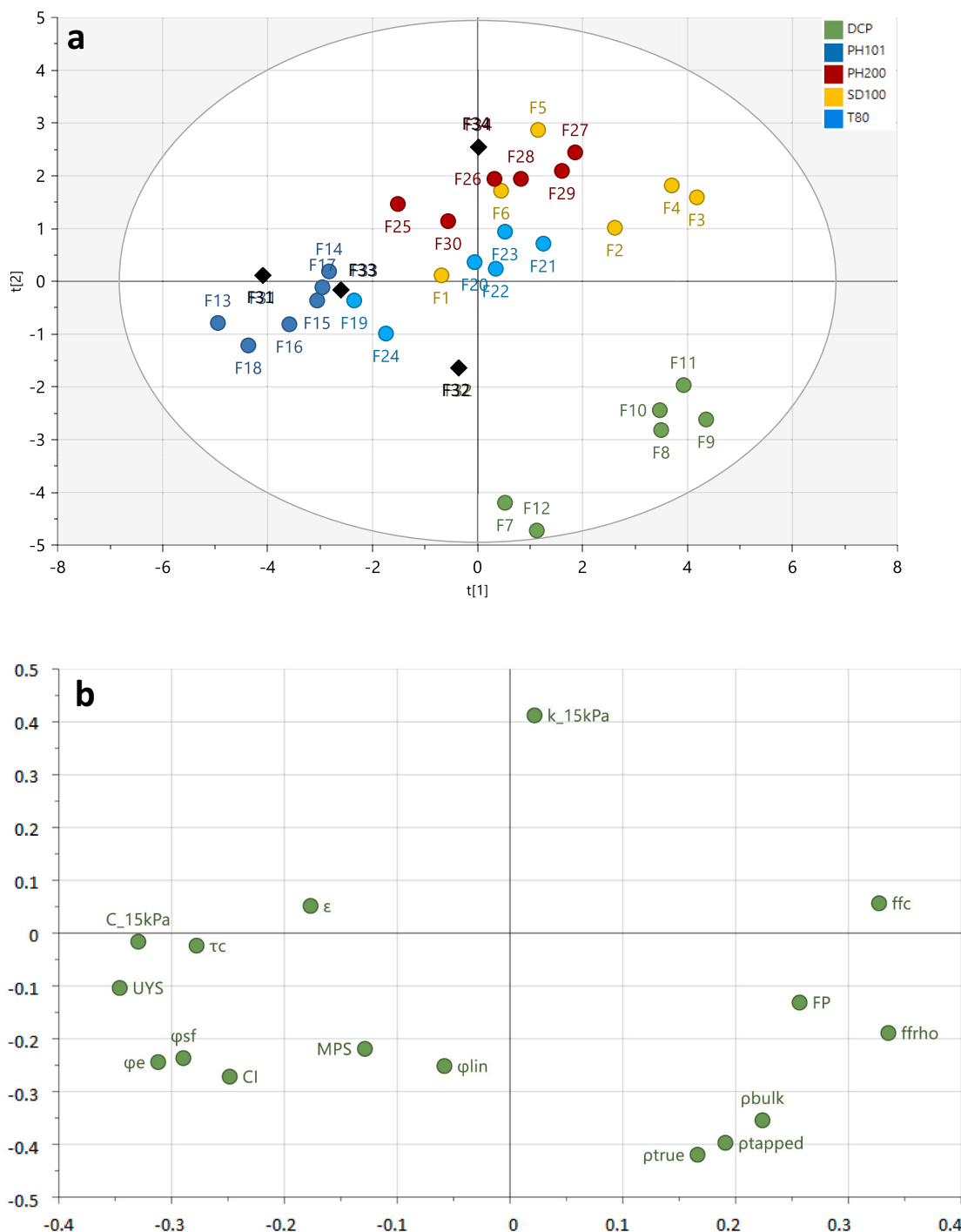


**Fig. 2.** PC 1 vs PC 2 scores (a) and loadings (b) plot of the characterized blends. Blends are colored according to their filler. External validation blends are marked with a black diamond.

Each spectrum was collected using 16 scans without attenuator and a detector gain of 100. In total 75 pre-processed spectra (5 calibration standards x 5 tablets/calibration standard x 3 thicknesses) were regressed with their corresponding concentration via PLS regression using SIMCA 16 software (Umetrics AB, Umeå, Sweden). The root mean squared error of cross validation (RMSEcv) was used as an indicator for the model performance.

### 4.4.2. Off-line verification

Off-line UV-VIS and HPLC analysis was performed on a subset of tablets as an analytical reference method to verify the API concentrations determined via in-line NIR (i.e. SentroPAT FO and Lighthouse™ probe) and off-line NIR transmission spectroscopy (i.e. Antaris™ II FT-NIR Analyzer). The subset of tablets were selected at random from both good (i.e. F9 and F15) and poorly (i.e. F7 and F13) flowing blends as well as tablets from runs with API_sd (i.e. F5, F11, F17, F23 and F29). An in-house HPLC method was applied for the analysis of tablets containing API_sd. Tablets containing a paracetamol grade (i.e. P_P, P_DP, P_μ) were analyzed via UV-VIS analysis. One tablet (i.e. 175 mg) was homogenized in 50 mL distilled water, diluted 1/50 and measured at a wavelength of 243 nm using a UV spectrophotometer with a 1 cm cell (Shimadzu UV-1650PC, Shimadzu Corporation, Kyoto, Japan). The API concentration was determined via calibration curves which were developed through the analysis of the calibration standards of the selected blends (cf. 4.3.2 Blend uniformity calibration models).

## 5. Results and discussion

### 5.1. Blend selection and characterization

The blend characterization resulted in a principle component analysis (PCA) model with a goodness of fit ($R^2X$) and prediction ($Q^2$) of 85.4% and 69.2%, respectively. Based on the blend properties, the relationship of the blends to each other is depicted by the scores plot (Fig. 2a) and correlations between the blend properties are revealed in the loadings plot (Fig. 2b). Both plots can be superimposed, revealing that blends with a similar location as properties on the loadings plot have high values for that property and low values for those at the opposite side of the origin. The clustering of the blends in the scores plot suggested a high contribution from the filler properties. In each cluster, a separation (i.e. along the x-axis; principle component 1) could be seen for the blends containing the highly cohesive and compressible APIs (i.e. MPT_μ and P_μ), indicating the impact of highly cohesive and compressible APIs on the overall blend. Blends containing DCP as filler (i.e. green dots) showed a clear separation from the other blends along the y-axis (i.e. principle component 2), suggesting that density was an important differentiator.

Overall, the chosen descriptors could be used to make differentiations between the blends, where principle component 1 (PC1) explained the variability in flowability and compressibility, while principle component 2 (PC2) showed the effect of the permeability and density of a blend.

### 5.2. CDC-50 trials

### 5.2.1. Blend processability

The CDC-50 trials revealed some challenges regarding the processability of the materials in different unit operations. During the feeding process several difficulties/limitations were observed when the process was run for longer periods of time (e.g. bridging, layering…), which had a negative impact on the down-stream unit operations. These problems were mainly related to the flowability and compressibility of the raw materials. These processability issues and their correlations with the material properties were described by Bekaert et al. (2021c).

For the blending step, both the main and lubricant blender exhibited limited processability difficulties for most of the selected blends.

However, layering of the paddles for cohesive materials (i.e. P_μ, MPT_μ, C_P and P_P) was observed throughout the process (Fig. 3). The degree of layering was dependent on the cohesivity of the materials in the blend, where blends containing P_μ and MPT_μ exhibited the highest layering potential. This layering could manifest problems related to blend uniformity for blends with a low content of the layered material, due to the relatively higher API loss on the paddles.

During the tableting process several problems were observed related to the blend composition, which required an adjustment in composition or ultimately the removal of several blends from the experimental plan. Firstly, the ratio of blends containing Pearlitol 100 SD (SD100) was adjusted to a higher lubricant concentration (i.e. from 0.75% to 1.25%) in order to reduce the capping potential of the tablets. Capping (Fig. 4a) occurred due to the high ejection forces which was caused by the brittle fracture nature of mannitol (Mohan, 2012). Brittle particles will break up, creating new unlubricated particle surfaces, which can induce higher ejection forces. Therefore, an increase in lubricant concentration should cover more unlubricated surfaces (Mohan, 2012). Secondly, the cohesive nature of particular blends (i.e. F6 – MPT_μ + SD100; F12 – MPT_μ + DCP; F24 – MPT_μ + T80) led to their removal from the experimental plan, since it was not possible to make tablets. Punch-sticking of MPT_μ combined with the brittle nature of SD100 and T80 resulted in broken tablets at the ejection chute. Furthermore, the low target tablet weight (i.e. 175 mg) generated thin tablets when dense fillers (i.e. DCP) were used (Fig. 4b). This phenomenon combined with punch-sticking of MPT_μ led to tablets that were broken easily during ejection. However, the punch-sticking phenomenon of MPT_μ was reduced through the addition of plastically deforming fillers (i.e. PH101 and PH200), making it possible to produce tablets.

### 5.2.2. Predictive model

The CDC-50 trials generated both blending (i.e. $HM_1$, $BRT_1$ and $\#BP_1$) and compression (i.e. FD, PCH, MCH, $\sigma_{Force}$, $\sigma_{PCD}$ and $RSD_{TW}$) responses which were included into one PLS model with three principle components (PC) and a goodness of fit ($R^2Y$) and prediction ($Q^2$) of 78.7% and 77.7%, respectively. Blend and content uniformity responses were not included due to their limited goodness of fit and predictive performance (i.e. $R^2Y < 16\%$ and $Q^2 < 12\%$). Additionally, data from the blends F6, F12 and F24 were excluded due to processability issues. The $R^2Y$ and $Q^2$ for each response is displayed in Table 6. Any correlation between the blend properties, process settings and process responses were established through the scores and loadings plots (i.e. PC1 vs. PC2 and PC1 vs. PC3) depicted in Fig. 5. The scores-plot showed that the data corresponding to blend F7 (i.e. P_μ + DCP) were outside the



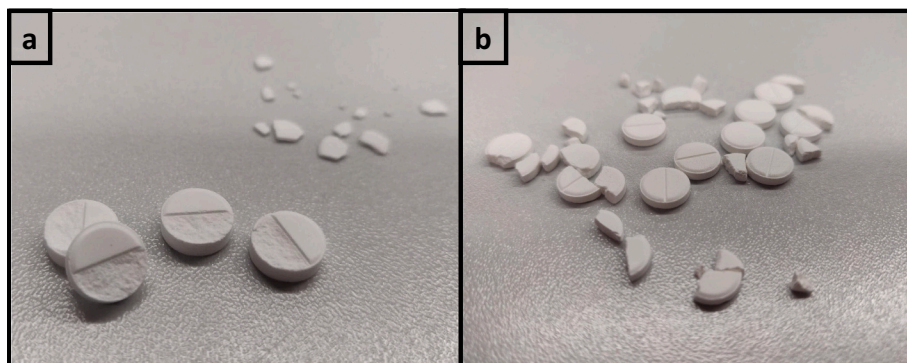**Fig. 3.** Layering of P_P on the impeller shaft and paddles.

**Fig. 4.** (a) Tablets produced with blend F2 (i.e. P_P + SD100) during the CDC-50 trials exhibiting capping. (b) Thin tablets produced with blend F9 (i.e. P_DP + DCP) which were prone to breakage.

**Table 6**
Overview of the constructed PLS model. $R^2Y$ and $Q^2$ are given for the overall model and all responses.

| Overal model | | |
|---|---|---|
| #PC | $R^2Y$ | $Q^2$ |
| 1 | 0.307 | 0.303 |
| 2 | 0.524 | 0.512 |
| 3 | 0.787 | 0.777 |
| **Blending responses** | | |
| Name | $R^2Y$ | $Q^2$ |
| $HM_1$ | 0.856 | 0.842 |
| $BRT_1$ | 0.856 | 0.842 |
| $\#BP_1$ | 0.827 | 0.818 |
| **Compression responses** | | |
| FD | 0.804 | 0.801 |
| PCH | 0.856 | 0.848 |
| MCH | 0.601 | 0.594 |
| $\sigma_{force}$ | 0.736 | 0.714 |
| $\sigma_{PCD}$ | 0.811 | 0.803 |
| $RSD_{TW}$ | 0.729 | 0.715 |

95% confidence level. However, these datapoints were not excluded in order to increase the predictive performance of the model. Additionally, coefficient plots were used to gain a better insight into the significance of the correlations using a 95% confidence level.

*5.2.2.1. Blending responses.* High $R^2Y$ and $Q^2$ values were observed for the three collected blending responses (i.e. $HM_1$, $BRT_1$ and $\#BP_1$) (Table 6), suggesting a high predictive performance of the model. A close correlation between the responses was observed (i.e. located close to each other on the loadings plot) since the equations for $BRT_1$ (Eq. (1)) and $\#BP_1$ (Eq. (2)) were both derived from $HM_1$. Looking at the loadings plot for PC1 vs PC2 (Fig. 5b), the blending response cluster and process settings (i.e. number of radial mixing blades ($\#RMB_1$); and impeller speed ($Imp_1$)) were located relatively close to the origin and away from the blend property descriptors. This indicated that a limited correlation with the material properties, which was confirmed by the coefficient plot for $BRT_1$ where the density-related descriptors (i.e. ρb, ρt, CBD) and porosity exhibited a direct and inverse correlation, respectively. These correlations could be explained by the fact that a certain blender fill level was required for the impeller blades to transport the material. Therefore, dense materials will have a larger hold-up mass for the same blender fill level compared to a less dense material.

The separation between blend properties and process settings was clearly visualized by the loadings plot for PC1 vs PC3 (Fig. 5c). The blending process was mainly correlated with the number of radial mixing blades ($\#RMB_1$) and impeller speed ($Imp_1$). The positive correlation with $\#RMB_1$ was caused by an increase in radial mixing potential

due to the higher number of radial mixing blades, while less transport blades were available to push the blend forward. Therefore, more material was present in the blender at the same time, increasing the hold-up mass. Furthermore, the inverse correlation with $Imp_1$ was attributed to the increased powder movement at higher impeller speed. A faster powder movement resulted in less material in the blender and consequently a lower hold-up mass.

Overall, these observations elucidated that the blending responses of divergent blends in the fully optimized and integrated CDC-50 blender setup was mainly dependent on process parameters (i.e. impeller speed) and equipment configurations (i.e. number of radial mixing blades). Furthermore, only limited blend properties (i.e. density-related descriptors) could be varied in order to change the blending responses.

*5.2.2.2. Compression responses.* Based on the location on the loadings plot (Fig. 5b), two clusters related to the compression step were found. The first comprised the tablet press settings (i.e. FD, PCH and MCH) needed to reach a tablet weight of 175 mg, pre-compression force of 1.5 kN and main compression force of 5 kN at a throughput of 20 kg/h. The location of the required fill depth (FD) at the positive side of PC1 (right side) indicated a positive correlation with the blend properties describing a poorly flowing (i.e. Cohesion, UYS), highly compressible (i. e. C_15kPa), friction generating (i.e. $\phi_e$, $\phi_{sf}$) and porous (ε) blend. The irregular flow behavior of such blends resulted in a poor and inconsistent die filling of the narrow die cavities, requiring a larger fill depth in order to cope with the variability (Mehrotra et al., 2009; Mendez et al., 2012; Peeters et al., 2015; Sinka et al., 2004; Sun, 2010; Van Snick et al., 2017a; Van Snick et al., 2018; Yaginuma et al., 2007). Blends with high porosity were also highly compressible, resulting in an inconsistent die filling. Therefore, properties describing a consistent die filling (i.e. high flowability; ffc, ffp and FR) were located at the opposite side along PC1. The density (i.e. ρb, ρt, $\rho_{true}$ and CBD) of a blend also impacted the fill depth: smaller fill depths were sufficient for denser materials to reach the specified tablet weight. The positive correlation of permeability (i.e. k_15kPa) along PC2 (y-axis) was attributed to the larger volume of highly permeable blends, thus requiring a larger fill depth. Furthermore, an inverse relationship of wall friction (i.e. WFA) was seen which could be attributed to the fact that highly porous materials tended to have a lower WFA (i.e. PH101 and PH200). Similar observations were seen for the remaining tablet press settings (i.e. MCH and PCH) located close to FD, indicating a close correlation with each other. This correlation was attributed to the dependency of MCH and PCH to the fill depth, since an adjustment in fill depth required a change in PCH and MCH in order to reach the required compression forces. Furthermore, no influence from the blending process was observed, based on the location of the blending descriptors (i.e. $\#RMB_1$ and $Imp_1$) close to the origin in the loadings plot for PC1 vs PC2 (Fig. 5b) and through their separation in the loadings plot for PC1 vs PC3 (Fig. 5c).
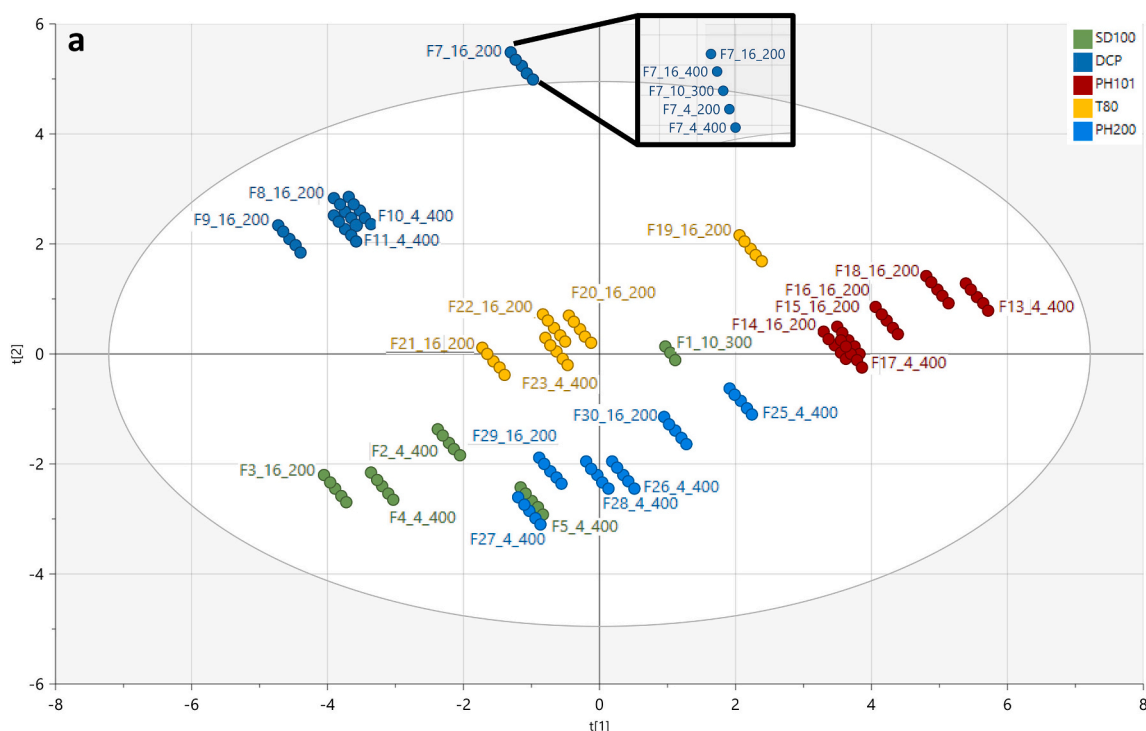
**Fig. 5.** Scores and loadings plots of the overall PLS model with: (a) PC 1 vs PC 2 scores and (b) loadings plot; (c) PC 1 vs PC 3 loadings plot. Blends are colored according to their filler. The naming consists of the blend name followed by the $\#RMB_1$ and $Imp_1$ (e.g. _10_300 = 10 RMB at 300 rpm). Score plot labels were removed to increase visibility. The enlargement of one cluster is a representation of the location for each trial run in a cluster.

The second cluster contained the compression (i.e. $\sigma_{Force}$, $\sigma_{PCD}$) and tablet (i.e. $RSD_{TW}$) responses (Fig. 5b). These responses described the variability introduced by the blends during the compression process once the target settings (i.e. tablet weight, PCD, PCF and MCF) were achieved. A limited and insignificant impact of the blending descriptors (i.e. located close to the origin) was observed, whereas the die filling consistency could be seen as the main contributor for the compression and tablet responses. Therefore, all responses in the cluster showed similar correlations with the blend properties related to die filling: flowability (ffc, ffp and FR), cohesion (cohesion, UYS, MPS), friction ($\phi_e$, $\phi_{sf}$), compressibility (C_15kPa), density ($\rho b$, $\rho t$, $\rho_{true}$ and CBD), porosity ($\varepsilon$) and WFA. A lower variability (i.e. inverse correlation; at the opposite side of the loadings plot) was observed for good flowing and dense blends since these exhibit an easy and consistent die filling potential. On the other hand, materials with a high cohesivity, friction and compressibility reduced the powder flow. Similar observations were made by Van Snick et al. (2018) where batch-wise blending was performed prior to compression instead of continuous blending, thus confirming their conclusions on the impact of die filling on the compression step.

Overall, the descriptors for the compression step had a high goodness of fit ($R^2Y$) and predictive ability ($Q^2$) (Table 6), which was calculated via internal cross validation. These observations elucidated the potential to predict the processability of a new blend on the CDC-50.

### 5.2.3. Model validation

The four new ternary blends (Table 5) were characterized for the same descriptors as the trial blends and included into the blend characterization PCA model (Fig. 2). The data from the processed validation blends on the CDC-50 were compared with the values predicted by the model. An overview of the observed and predicted values, combined with the calculated prediction errors, is given in Table 7. The table could be divided into three sections: process settings (i.e. FD, PCH and MCH), blender responses (i.e. $HM_1$, $BRT_1$ and $\#BP_1$) and compression ($\sigma_{Force}$,

$\sigma_{PCD}$) and tablet responses (i.e. $RSD_{TW}$).

Blend F31 (i.e. T_P + PH101 + MgSt) which was the blend with a new API in the same API ratio as the trial blends, exhibited a high predictive performance (i.e. < 30% $Error_{Rel}$) for the process settings and the blender responses (i.e. $HM_1$, $BRT_1$ and $\#BP_1$). However, an overprediction for the compression and tablet responses was seen, resulting in a larger predictive error (30% < $Error_{Rel}$ < 60%). The larger error could originate from the variability in tablet weight during compression. Theoretically, the tablet weight was fixed at 175 mg, but during steady state small changes in powder flow/die filling could result in an altered tablet weight. These changes in tablet weight influence the compression and tablet responses and are unpredictable, thus reducing the prediction of these responses. Blend F32 exhibited larger predictive errors for the process settings and blender responses compared to blend F31. Additionally a very poor predictive performance for the compression and tablet responses was observed. These observations could be explained by the fact that, compared to the location of F31 inside the overall blend cluster, F32 was located between both filler clusters in an untested region (Fig. 2), hence the developed prediction model does not contain sufficient data to make accurate predictions. Therefore, continuous model learning has to be applied where the gaps in the model (e.g. blends outside of the blend space; blends located inside the blend space, but in areas with little to no available data) are filled through the addition of new experimental data. The need for continuous model learning was also visible for the blends with an altered blend-ratio (i.e. F33 and F34) for which similar prediction error values were observed.

Overall, a good predictability for the process settings and blending step was achieved for new blends with the same API ratio located inside the PCA cluster. Based on the larger prediction errors for blends in untested areas of the PCA cluster or blends with different ratios, additional dedicated experimental trials are required using divergent blend compositions. The reduced predictive performance (i.e. larger prediction errors) is a typical disadvantage of the empirical models used during this study. This could be improved by applying pure mechanistic models.
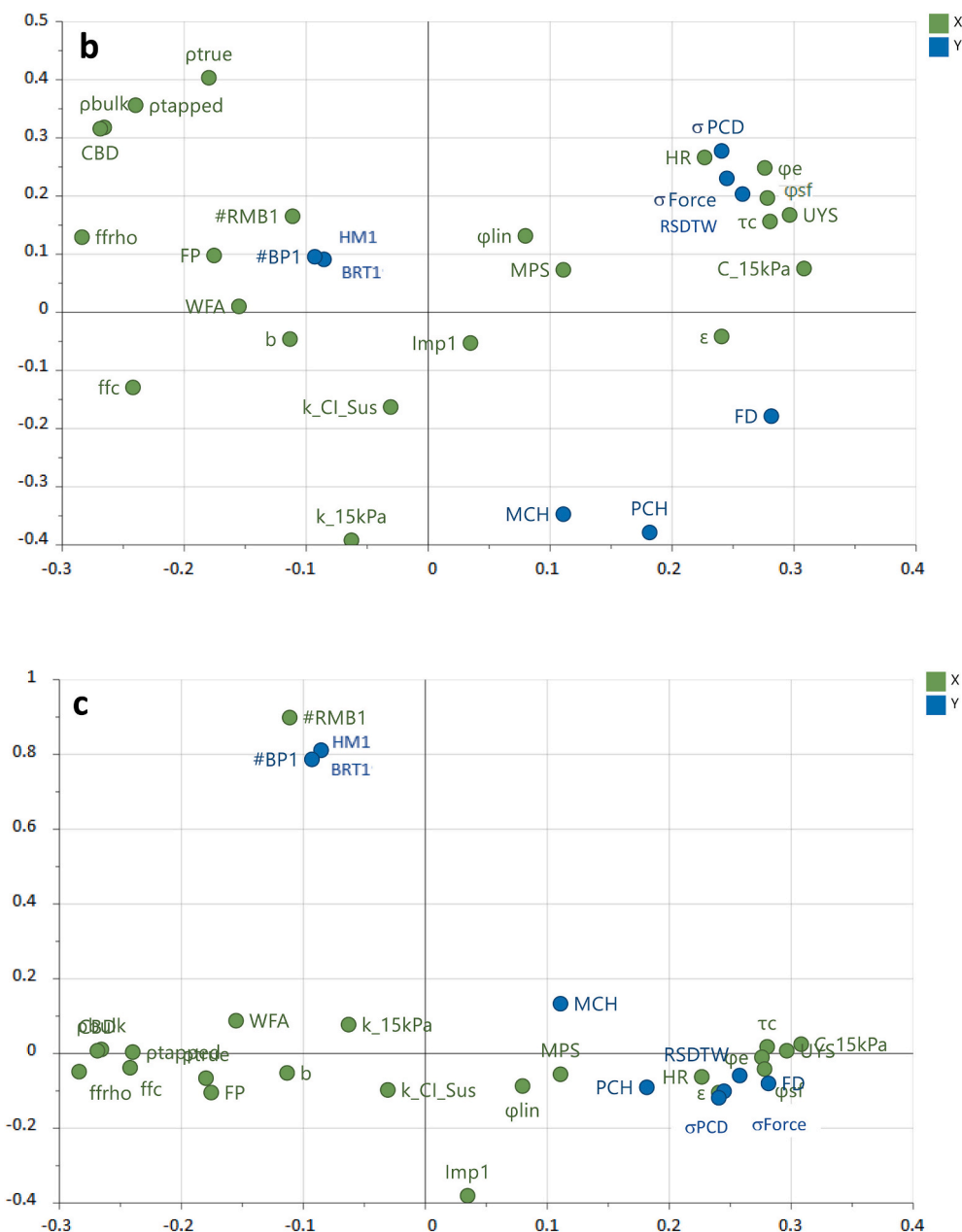
**Fig. 5.** (*continued*).

However, such models make a lot of assumptions (Nestorov et al., 2019). An additional disadvantage for both models is the inability to cope with non-linear phenomena which could be solved using neural networks (Thakur, 1991; Wong et al., 2018). Taking the different modeling techniques into consideration combined with continuous model learning could further improve the predictive performance for the blending and compression step. However, based on the current predictive ability of the model, time needed to optimize the CDC-50 process could be reduced.

### 5.3. Blend uniformity

Fig. 6 gives an overview of the average blend uniformity label claim (LC) for each performed trial run measured by both NIR probes (i.e. Lighthouse™ and SentroPAT FO probe). Some datapoints are missing due to processability issues such as punch sticking and tablet capping. Based on the standard deviation of the measurement (i.e. 1.0 to 15.0%)

and the relative prediction error of the calibration models (i.e. 2.0 to 20.0%), most trial runs were able to contain the target concentration within their error bars. Furthermore, no statistically significant impact from the blender configurations and blender speeds on the label claim and its variability was observed, indicating a highly robust setup and confirming similar observations by Van Snick et al. (2017a).

Generally, the error bars of the SentroPAT FO predictions were larger compared to the Lighthouse™ probe, which could be attributed to the prediction error of the calibration models. Higher prediction errors were found for the SentroPAT FO models, since these were developed via off-line static measurements compared to the dynamic in-line models of the Lighthouse™ probe. Dynamic measurements take the powder flow and density changes during sample presentation into consideration, enhancing the predictive ability (i.e. lower prediction error) (European Pharmacopoeia, 2006). The absence of these phenomena during the development of the static calibration models of the SentroPAT FO probe could generate a larger variability in the BU measurement as well as

**Table 7**

Overview of the observed versus predicted values and corresponding prediction error for the model validation.

| Process settings | | | | | | | | | | | |
|---|---|---|---|---|---|---|---|---|---|---|---|
| Blend | $Imp_1$ | FD (mm) | | | PCH (mm) | | | MCH (mm) | | |
| | | Observed | Predicted | Error (%) | Observed | Predicted | Error (%) | Observed | Predicted | Error (%) |
| F31 | 200 | 9.80 | 9.74 | 0.58 | 5.67 | 5.73 | 0.97 | 4.77 | 4.93 | 3.38 |
| | 300 | 9.94 | 9.93 | 0.12 | 5.67 | 5.76 | 1.65 | 4.75 | 4.92 | 3.62 |
| | 400 | 9.80 | 10.12 | 3.23 | 5.63 | 5.80 | 3.05 | 4.75 | 4.91 | 3.43 |
| F32 | 200 | 3.99 | 3.82 | 4.37 | 4.37 | 4.86 | 11.19 | 4.11 | 4.53 | 10.12 |
| | 300 | 3.96 | 3.89 | 1.81 | 4.40 | 4.90 | 11.30 | 4.13 | 4.52 | 9.37 |
| | 400 | 3.92 | 3.96 | 1.07 | 4.37 | 4.94 | 12.94 | 4.11 | 4.51 | 9.68 |
| F33 | 200 | 6.52 | 7.60 | 16.54 | 5.59 | 5.46 | 2.40 | 4.95 | 4.81 | 2.82 |
| | 300 | 6.61 | 7.74 | 17.14 | 5.57 | 5.49 | 1.36 | 4.93 | 4.80 | 2.61 |
| | 400 | 6.67 | 7.89 | 18.29 | 5.59 | 5.53 | 1.02 | 4.94 | 4.79 | 2.99 |
| F34 | 200 | 6.05 | 7.75 | 28.04 | 5.61 | 5.73 | 2.23 | 4.94 | 5.03 | 1.86 |
| | 300 | 6.05 | 7.89 | 30.47 | 5.61 | 5.77 | 2.91 | 4.94 | 5.02 | 1.67 |
| | 400 | 6.12 | 8.04 | 31.43 | 5.58 | 5.81 | 4.15 | 4.92 | 5.01 | 1.90 |

| Blender responses | | | | | | | | | | | |
|---|---|---|---|---|---|---|---|---|---|---|---|
| Blend | $Imp_1$ | $HM_1$ (g) | | | $BRT_1$ (s) | | | $\#BP_1$ | | |
| | | Observed | Predicted | Error (%) | Observed | Predicted | Error (%) | Observed | Predicted | Error (%) |
| F31 | 200 | 332.3 | 303.1 | 8.77 | 59.8 | 54.6 | 8.77 | 199.4 | 244.8 | 22.80 |
| | 300 | 241.6 | 211.5 | 12.46 | 43.5 | 38.1 | 12.46 | 217.4 | 178.5 | 17.92 |
| | 400 | 182.0 | 147.6 | 18.92 | 32.8 | 26.6 | 18.92 | 218.4 | 130.1 | 40.43 |
| F32 | 200 | 1034.0 | 662.0 | 35.97 | 186.1 | 119.2 | 35.97 | 620.4 | 512.2 | 17.44 |
| | 300 | 273.4 | 461.9 | 68.95 | 49.2 | 83.1 | 68.95 | 246.1 | 373.4 | 51.73 |
| | 400 | 162.8 | 322.3 | 97.95 | 29.3 | 58.0 | 97.95 | 195.4 | 272.2 | 39.31 |
| F33 | 200 | 840.0 | 425.1 | 49.39 | 151.2 | 76.5 | 49.39 | 504.0 | 334.3 | 33.68 |
| | 300 | 459.2 | 296.6 | 35.41 | 82.7 | 53.4 | 35.41 | 413.3 | 243.7 | 41.04 |
| | 400 | 247.1 | 206.9 | 16.26 | 44.5 | 37.3 | 16.26 | 296.5 | 177.6 | 40.10 |
| F34 | 200 | 907.3 | 496.4 | 45.29 | 163.3 | 89.4 | 45.29 | 544.4 | 384.9 | 29.30 |
| | 300 | 284.2 | 346.3 | 21.86 | 51.2 | 62.3 | 21.86 | 255.8 | 280.6 | 9.68 |
| | 400 | 122.1 | 241.6 | 97.89 | 22.0 | 43.5 | 97.90 | 146.5 | 204.5 | 39.58 |

| Compression and tablet responses | | | | | | | | | | | |
|---|---|---|---|---|---|---|---|---|---|---|---|
| Blend | $Imp_1$ | $\sigma_{Force}$ (%) | | | $\sigma_{PCD}$ (%) | | | $RSD_{TW}$ (%) | | |
| | | Observed | Predicted | Error (%) | Observed | Predicted | Error (%) | Observed | Predicted | Error (%) |
| | 200 | 0.50 | 0.71 | 41.99 | 1.44 | 2.17 | 50.62 | 2.23 | 3.49 | 56.26 |
| F31 | 300 | 0.54 | 0.73 | 34.83 | 1.65 | 2.24 | 35.94 | 2.33 | 3.55 | 52.05 |
| | 400 | 0.55 | 0.75 | 35.76 | 1.65 | 2.32 | 40.59 | 2.26 | 3.61 | 59.46 |
| | 200 | 0.23 | 0.53 | 132.45 | 0.77 | 1.70 | 121.18 | 0.84 | 2.33 | 177.40 |
| F32 | 300 | 0.22 | 0.55 | 149.22 | 0.75 | 1.76 | 134.83 | 0.77 | 2.37 | 208.10 |
| | 400 | 0.25 | 0.56 | 124.91 | 0.75 | 1.82 | 142.85 | 0.74 | 2.41 | 225.05 |
| | 200 | 0.53 | 0.68 | 27.70 | 1.90 | 2.12 | 11.32 | 2.26 | 3.24 | 43.41 |
| F33 | 300 | 0.66 | 0.69 | 5.16 | 1.66 | 2.19 | 31.77 | 2.09 | 3.29 | 57.34 |
| | 400 | 0.80 | 0.71 | 11.03 | 2.11 | 2.26 | 7.21 | 2.12 | 3.35 | 58.15 |
| | 200 | 0.13 | 0.29 | 119.97 | 0.40 | 0.66 | 65.99 | 0.55 | 1.25 | 128.78 |
| F34 | 300 | 0.13 | 0.29 | 125.58 | 0.35 | 0.69 | 96.18 | 0.57 | 1.27 | 124.85 |
| | 400 | 0.18 | 0.30 | 67.08 | 0.34 | 0.71 | 108.85 | 0.55 | 1.29 | 133.90 |

result in under- or overpredictions of the actual blend uniformity. Due to the inaccessibility to the blender outlet during the process, no samples were taken of the blend. Therefore, under- or overpredictions were investigated via CU of the tablets (Fig. 6). Small differences between BU and CU could be due to further (de)mixing by the feed frame, but this would have a limited influence on the SentroPAT FO values, since BU was measured just before die-filling. An example of an underprediction can be seen for the blends containing P_DP and DCP where a significant difference was observed between the online measured BU and off-line measured CU via UV-VIS (Fig. 6c). This phenomenon could be explained by the combination of highly dense and good flowing powders, causing density changes during the BU measurement.

Furthermore, a formulation-dependent effect on the BU variability was observed where an increase in variability was present for blends containing a cohesive component (i.e. P_μ, P_P and MPT_μ blends; Fig. 6a,b,f). The cohesiveness of such formulations resulted in powder adhesion to the probe (i.e. window fouling) which artificially increased or decreased the concentration of the blend, resulting in a larger variability. Window fouling was visually observed throughout the experimental runs and could be resolved through frequent cleaning of the probes.

The phenomena of window fouling and changes in sample presentation (e.g. density changes, flow changes) indicate the need for proper implementation of the sensors in order to achieve a consistent and representative measurement. Therefore, further dedicated experiments are required to optimize the implementation of PAT-tools depending on the pharmaceutical process and processed powders.

### 5.4. Content uniformity

Based on the prediction error (i.e. 2.0 to 7.0%) and the standard deviation from the measurement (i.e. 1.0 to 14%), the error bars for most of the grab samples overlapped with the required content uniformity and could be linked to the blend uniformity measured just before die-filling (i.e. SentroPAT FO probe measurements). Due to the absence of window fouling, lower prediction errors were achieved. However, as
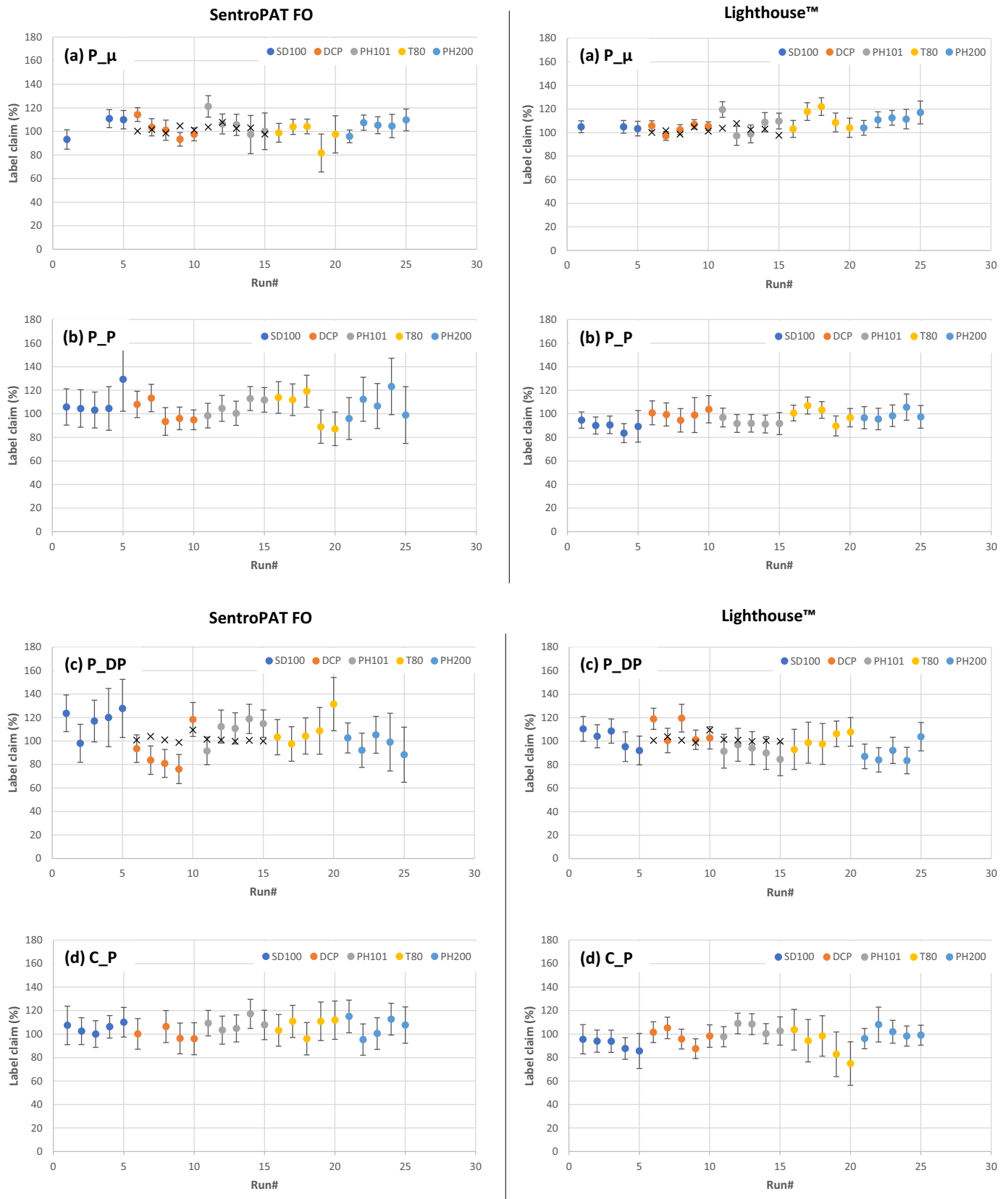
**Fig. 6.** Overview of the average BU label claim measured with the SentroPAT FO (left) and Lighthouse™ (right) probe for the trial runs with blends containing: (a) P_μ; (b) P_P; (c) P_DP; (d) C_P; (e) API_sd; (f) MPT_μ. Blends are colored according to the filler with in each color cluster from left to right the experimental run: 10_300; 16_200; 16_400; 4_200; 4_400. The different markings stand for: dot = label claim; cross = Off-line analysis.
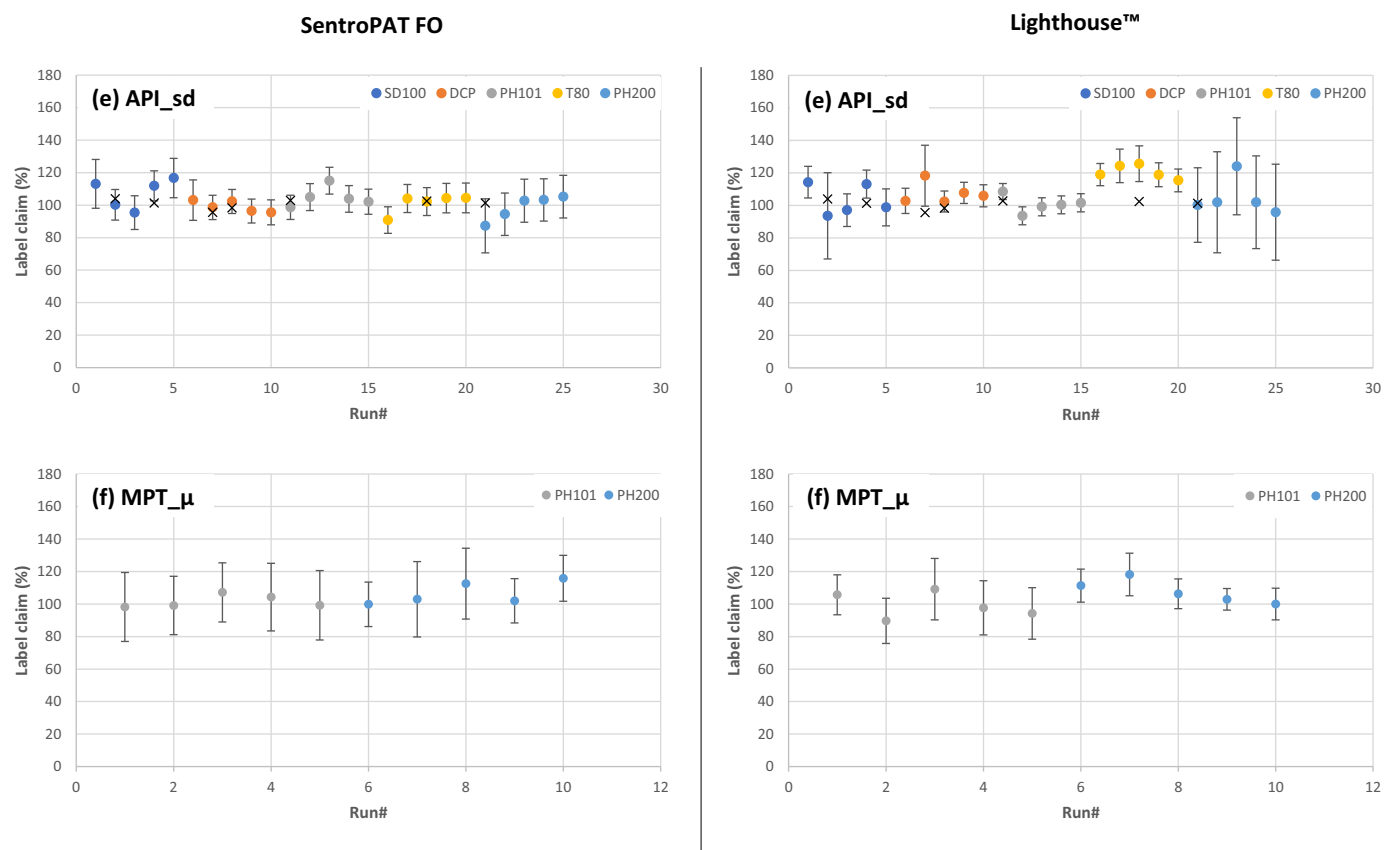
**Fig. 6.** (*continued*).

depicted in Fig. 7a, the content uniformity of tablets containing API_sd suggested that their API concentration was too high even though the blend uniformity indicated otherwise (Fig. 6e). In order to determine if the predictions were correct, off-line HPLC analysis was performed to determine the actual concentration in the tablets. Based on the off-line analysis (Figs. 6e and 7a), the tablets contained a lower concentration (i.e. similar to the BU measurement) than predicted. These observations indicated that the calibration model did not accurately predict the API concentration and a formulation-dependent CU measurement is needed.

Tablets containing highly cohesive materials (i.e. P_μ + PH101 and MPT_μ blends) exhibited a larger variability in API content (Fig. 7b) which could be attributed to punch-sticking (i.e. the cohesive API sticks to the punches) and/or inconsistent die-filling where a variable amount

of cohesive material is filled into the die (Van Snick et al., 2018). The effect of inconsistent die-filling was elucidated in Fig. 7b where the runs with a high RSD_TW, which is related to inconsistent die-filling, also exhibited larger CU variabilities.

Off-line UV-VIS analysis for tablets with the correct API content, confirmed that NIR transmission measurements were capable of predicting the actual content uniformity (Figs. 6a and 7b).

## 6. Conclusion

Formulations with cohesive/adhesive properties impacted the processability during both blending (i.e. impeller paddle layering) and compression (i.e. punch sticking) phases, resulting in the need for blend
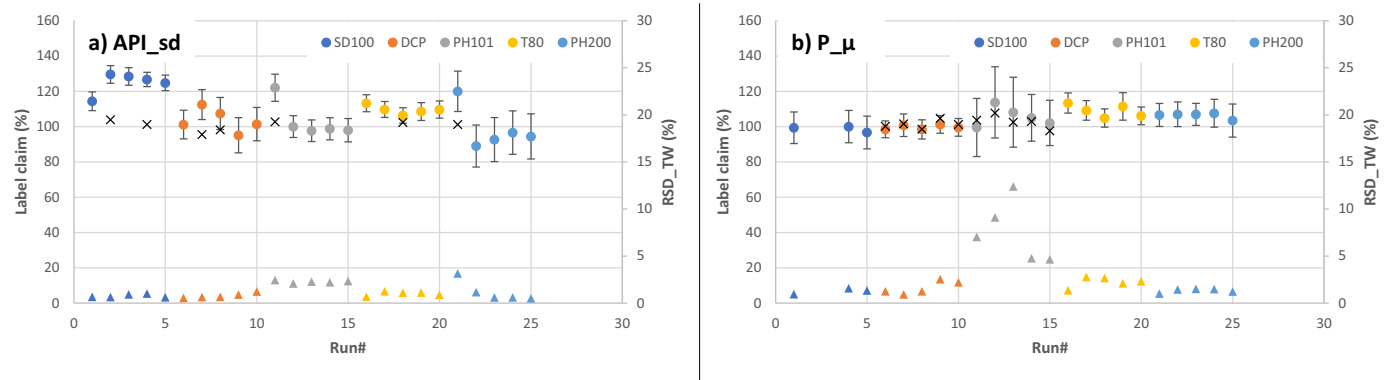


**Fig. 7.** Overview of the average CU label claim measured with the Antaris™ II FT-NIR Analyzer for the trial runs with blends containing: (a) API_sd and (b) P_μ. Blends are colored according to the filler with in each color cluster from left to right the experimental run: 10_300; 16_200; 16_400; 4_200; 4_400. The different markings stand for: dot = label claim; triangle = RSD_TW; cross = Off-line analysis.

composition changes. In addition, the brittle nature of some blends resulted in low quality tablets (i.e. capping). Quantitative relationships between blend properties and blending/compression CQAs and CPPs were established through PLS regression and were used to develop a predictive model. Clear correlations were found between the blending responses and blender configuration (i.e. #RMB$_1$ and Imp$_1$), suggesting a large freedom in configuration adjustments in order to acquire the desired blending responses. On the other hand, only limited correlations with the blend properties (i.e. density) were observed, indicating a robust blending setup with limited impact of blend properties. The compression step exhibited significant correlations with the blend properties related to a consistent die-filling process (i.e. flowability, compressibility, density and permeability) where an adjustment in blend composition could significantly alter the tablet quality. Secondly, further model optimization and learning is required in order to allow for more accurate predictions of deviating and challenging blends (e.g. blends at the edges of the model). Overall, the predictive model could reduce the number of trial runs needed to optimize a process (e.g. reduction or elimination of trial-and-error runs to determine the tablet press settings, such as FD, PCH and MCH, through the correlation between these parameters and the die-filling properties), this reducing the development time and cost of new drug products. Finally, blend and content uniformity measurements gave insights into the robustness of the process. Larger prediction errors as well as under- and over-predictions were seen for the BU measurements due to challenges regarding the probe implementation (i.e. inconsistent sample presentation and window fouling), resulting in measurements with a higher uncertainty. Furthermore, CU and off-line UV-VIS/HPLC analysis elucidated that a higher tablet weight variability (i.e. inconsistent die-filling) and the occurrence of punch sticking had a negative impact on CU.

## Declaration of Competing Interest

The authors declare that they have no known competing financial interests or personal relationships that could have appeared to influence the work reported in this paper.

## Acknowledgments

## References

Bekaert, B., et al., 2021a. Determination of a quantitative relationship between material properties, process settings and screw feeding behavior via multivariate data-analysis. Int. J. Pharmaceut. 602 https://doi.org/10.1016/j.ijpharm.2021.120603.

Bekaert, B., et al., 2021b. Unpublished results Impact of Blend Properties and Process Variables on the Blending Performance of a Generic Main Blender.

Bekaert, B., et al., 2021c. Unpublished results In-Depth Analysis of the Long-Term Processability of Materials during Continuous Feeding.

Bohle, L.B., 2019. L.B. Bohle QBCON [WWW Document]. L.B. Bohle. Available from: https://www.continuous-production.com/continuous-manufacturing (accessed 05.3.19).

Bostijn, N., et al., 2019. A multivariate approach to predict the volumetric and gravimetric feeding behavior of a low feed rate feeder based on raw material properties. Int. J. Pharmaceut. 557 (December 2018), 342–353 [Internet]. Available from: https://doi.org/10.1016/j.ijpharm.2018.12.066.

Eli Lilly, 2018. Lilly to Present Clinical Data for Verzenio [WWW Document]. Eli Lilly. URL. https://investor.lilly.com/news-releases/news-release-details/lilly-present-clinical-data-verzenior-abemaciclib-and-real-world.

Engisch, W.E., Muzzio, F.J., 2014. Loss-in-weight feeding trials case study: pharmaceutical formulation. J. Pharm. Innov. 10 (1).

European Pharmacopoeia, 2006. 2.2.40 Near-Infrared Spectrophotometry, 5.0.

Galbraith, S.C., et al., 2019. Integrated modeling of a continuous direct compression tablet manufacturing process: a production scale case study. Powder Technol. [Internet] 354, 199–210. Available from: https://doi.org/10.1016/j.powtec.2019.05.078.

Galbraith, S.C., et al., 2020. Linking process variables to residence time distribution in a hybrid flowsheet model for continuous direct compression. Chem. Eng. Res. Des.

[Internet] 153, 85–95. Available from: https://doi.org/10.1016/j.cherd.2019.10.026.

Gao, Y., et al., 2011. Characterizing continuous powder mixing using residence time distribution. Chem. Eng. Sci. 66, 417–425. https://doi.org/10.1016/j.ces.2010.10.045.

García-Muñoz, et al., 2017. A flowsheet model for the development of a continuous process for pharmaceutical tablets: an industrial perspective. AICHE J. 64, 511–525. https://doi.org/10.1002/aic.15967.

Ierapetritou, M., Muzzio, F., Reklaitis, G., 2016. Perspectives on the continuous manufacturing of powder-based pharmaceutical processes. AICHE J. 62, 1846–1862. https://doi.org/10.1002/aic.15210.

Järvinen, K., et al., 2013a. In-line monitoring of the drug content of powder mixtures and tablets by near-infrared spectroscopy during the continuous direct compression tableting process. Eur. J. Pharm. Sci. 48, 680–688. https://doi.org/10.1016/j.ejps.2012.12.032.

Järvinen, M.A., et al., 2013b. Continuous direct tablet compression: effects of impeller rotation rate, total feed rate and drug content on the tablet properties and drug release. Drug Dev. Ind. Pharm. 39, 1802–1808. https://doi.org/10.3109/03639045.2012.738681.

Lee, S.L., O'Connor, et al., 2015. Modernizing pharmaceutical manufacturing: from batch to continuous production. J. Pharm. Innov. 10, 191–199. https://doi.org/10.1007/s12247-015-9215-8.

Manufacturing Chemist, 2017. P-MEC 2017: Partnership to Develop Continuous Manufacturing Solutions [WWW Document]. Manuf. Chem. URL. https://www.manufacturingchemist.com/news/article_page/PMEC_2017_partnership_to_develop_continuous_manufacturing_solutions/137492.

Mehrotra, A., et al., 2009. A modeling approach for understanding effects of powder flow properties on tablet weight variability. Powder Technol. 188, 295–300. https://doi.org/10.1016/j.powtec.2008.05.016.

Mendez, R., Velazquez, C., Muzzio, F.J., 2012. Effect of feed frame design and operating parameters on powder attrition, particle breakage, and powder properties. Powder Technol. 229, 253–260. https://doi.org/10.1016/j.powtec.2012.06.045.

Mohan, S., 2012. Compression physics of pharmaceutical powders: a review. Int. J. Pharm. Sci. Res. 3 (6), 1580.

Nasr, M.M., Krumme, M., et al., 2017. Regulatory Perspectives on Continuous Pharmaceutical Manufacturing: moving from Theory to Practice: September 26-27, 2016, International Symposium on the Continuous Manufacturing of Pharmaceuticals. J. Pharm. Sci. 106, 3199–3206. https://doi.org/10.1016/j.xphs.2017.06.015.

Nestorov, I., Rowland, M., Hadjitodorov, S.T., et al., 2019. Empirical versus mechanistic modelling: Comparison of an artificial neural network to a mechanistically based model for quantitative structure pharmacokinetic relationships of a homologous series of barbiturates. AAPS PharmSci 1, 5–13. https://doi.org/10.1208/ps010417.

Osorio, J.G., Muzzio, F.J., 2016. Effects of processing parameters and blade patterns on continuous pharmaceutical powder mixing. Chem. Eng. Process. Process Intensif. 109, 59–67.

Patel, S., Kaushal, A.M., Bansal, A.K., 2006. Compression physics in the formulation development of tablets. Crit. Rev. Ther. Drug Carrier Syst. 23, 1–65.

Pawar, P., et al., 2016. Enabling real time release testing by NIR prediction of dissolution of tablets made by continuous direct compression (CDC). Int. J. Pharmaceut. 512, 96–107. https://doi.org/10.1016/j.ijpharm.2016.08.033.

Peeters, E., et al., 2015. Reduction of tablet weight variability by optimizing paddle speed in the forced feeder of a high-speed rotary tablet press. Drug Dev. Ind. Pharm. 41, 530–539. https://doi.org/10.3109/03639045.2014.884121.

Peeters, E., et al., 2018. Influence of extended dwell time during pre- and main compression on the properties of ibuprofen tablets. Eur. J. Pharm. Biopharm. 128 (2018), 300–315.

Pernenkil, L., Cooney, C.L., 2006. A review on the continuous blending of powders. Chem. Eng. Sci. 61, 720–742. https://doi.org/10.1016/j.ces.2005.06.016.

Pharmaceutical Technology, 2016. FDA Approves Tablet Production on Janssen Continuous Manufacturing Line. PharmaTech.Com, p. 312414. https://doi.org/10.1016/j.ijheatmasstransfer.2014.03.011. April 12.

Portier, C., Pandelaere, K., Delaet, U., Vigh, T., Di Pretoro, G., Vervaet, C., Vanhoorne, V., 2020. Continuous twin screw granulation: influence of process and formulation variables on granule quality attributes of model formulations. Int. J. Pharmaceut. https://doi.org/10.1016/j.ijpharm.2019.118981.

Portillo, P.M., Ierapetritou, M.G., Muzzio, F.J., 2008. Characterization of continuous convective powder mixing processes. Powder Technol. 182, 368–378. https://doi.org/10.1016/j.powtec.2007.06.024.

Roth, W.J., Almaya, A., Kramer, T.T., Hofer, J.D., 2017. A demonstration of mixing robustness in a direct compression continuous manufacturing process. J. Pharm. Sci. [Internet] 106 (5), 1339–1346. Available from: https://doi.org/10.1016/j.xphs.2017.01.021.

Schaber, S.D., et al., 2011. Economic analysis of integrated continuous and batch pharmaceutical manufacturing: a case study. Ind. Eng. Chem. Res. 50, 10083–10092. https://doi.org/10.1021/ie2006752.

Simonaho, S.-P., et al., 2016. Continuous manufacturing of tablets with PROMIS-line - Introduction and case studies from continuous feeding, blending and tableting. Eur. J. Pharm. Sci. 90 (2016), 38–46. ISSN 0928-0987. https://doi.org/10.1016/j.ejps.2016.02.006.

Sinka, I.C., Schneider, L.C.R., Cocks, A.C.F., 2004. Measurement of the flow properties of powders with special reference to die fill. Int. J. Pharmaceut. 280, 27–38. https://doi.org/10.1016/j.ijpharm.2004.04.021.

Sun, C.C., 2010. Setting the bar for powder flow properties in successful high speed tableting. Powder Technol. 201, 106–108. https://doi.org/10.1016/j.powtec.2010.03.011.

Thakur, A.K., 1991. Model: mechanistic vs. empirical. In: Rescigno, A., Thakur, A.K. (Eds.), New Trends in Pharmacokinetics. Plenum Press, New York, pp. 41–51.

U.S. Food and Drug Administration, 2018a. FDA Approves New Treatment for Patients with Acute Myeloid Leukemia [WWW Document]. Case Med. Res. https://doi.org/10.31525/fda2-ucm626443.htm.

U.S. Food and Drug Administration, 2018b. FDA Approves Lorlatinib for Second- or Third-Line Treatment of ALK-Positive Metastatic NSCLC [WWW Document]. Case Med. Res. https://doi.org/10.31525/fda1-ucm625027.htm.

U.S. Food and Drug Administration, 2018c. FDA Approves Abemaciclib as Initial Therapy for HR-Positive, HER2-Negative Metastatic Breast Cancer [WWW Document]. URL. https://www.fda.gov/drugs/resources-information-approved-drugs/fda-approves-abemaciclib-initial-therapy-hr-positive-her2-negative-metastatic-breast-cancer.

U.S. Food and Drug Administration, 2019. FDA Approves New Breakthrough Therapy for Cystic Fibrosis [WWW Document]. URL. https://www.fda.gov/news-events/press-announcements/fda-approves-new-breakthrough-therapy-cystic-fibrosis.

Van Snick, B., 2019. Experimental and Model-Based Analysis of a Continuous Direct Compression Platform for Oral Solid Dosage Manufacturing. [Ghent, Belgium]. Ghent University. Faculty of Pharmaceutical Sciences. http://hdl.handle.net/1854/LU-8610640.

Van Snick, B., et al., 2017a. Continuous direct compression as manufacturing platform for sustained release tablets. Int. J. Pharmaceut. 519 https://doi.org/10.1016/j.ijpharm.2017.01.010.

Van Snick, B., et al., 2017b. Development of a continuous direct compression platform for low-dose drug products. Int. J. Pharmaceut. 529 https://doi.org/10.1016/j.ijpharm.2017.07.003.

Van Snick, B., et al., 2018. Impact of blend properties on die filling during tableting. Int. J. Pharmaceut. 549 (1–2), 476–488. https://doi.org/10.1016/j.ijpharm.2018.08.015. Oct 5.

Van Snick, B., et al., 2019. Impact of material properties and process variables on the residence time distribution in twin screw feeding equipment. Int. J. Pharmaceut. 556, 200–216.

Wong, Wee Chin, et al., 2018. Recurrent neural network-based model predictive control for continuous pharmaceutical manufacturing. Mathematics 6 (11), 242.

Yaginuma, Y., et al., 2007. Effects of powder flowability on die-fill properties in rotary compression. J. Drug Deliv. Sci. Technol. 17, 205–210. https://doi.org/10.1016/S1773-2247(07)50037-7.